Published in final edited form as:

Nat Med. 2012 July ; 18(7): 1148–1153. doi:10.1038/nm.2821.

Fast degrading elastomer enables rapid remodeling of a cell-free synthetic graft into a neo-artery

Wei Wu[1,2], **Robert A. Allen**[1], and **Yadong Wang**[1,3,4]

[1]Department of Bioengineering, University of Pittsburgh, Pittsburgh, PA, USA

[2]Department of Maxillofacial Surgery, Qindu Hospital, Fourth Military Medical University, Xian, China

[3]Department of Surgery, University of Pittsburgh, Pittsburgh, PA, USA

[4]McGowan Institute for Regenerative Medicine, University of Pittsburgh, Pittsburgh, PA, USA

Abstract

Host remodeling is important for the success of medical implants including vascular substitutes. Synthetic and tissue-engineered grafts have yet to show clinical effectiveness in arteries smaller than 5 mm. We designed cell-free biodegradable elastomeric grafts that degrade rapidly to yield neo-arteries nearly free of foreign materials 3 months after interposition grafting in rat abdominal aorta. This design focuses on enabling rapid host remodeling. Three months post-implantation, the neo-arteries resemble native arteries in the following aspects: regular, strong and synchronous pulsation, a confluent endothelium and contractile smooth muscle layers, co-expression of elastin, collagen and glycosaminoglycan, and tough and compliant mechanical properties. Therefore, future study employing large animal models more representative of human vascular regeneration is warranted before clinical translation. This cell-free approach represents a philosophical shift from the prevailing focus on cells in vascular tissue engineering, and may impact regenerative medicine in general.

INTRODUCTION

A key challenge of arterial substitutes is that they need to withstand arterial pressure immediately upon implantation[1]. Naturally, the classic approaches to arterial substitutes use strong materials. This is reflected in autografts, synthetic grafts, and many tissue-engineered grafts[1–7]. Tissue-engineered grafts typically exhibit limited host cell infiltration and remodeling even 6–12 months post-implantation[8–11]. In vascular extracellular matrix (ECM), collagen provides strength and elastin provides elastic recoil. Collagen expression is typically very high for existing vascular grafts whereas elastin expression is usually

Correspondence should be addressed to Y.W. (yaw20@pitt.edu).

AUTHOR CONTRIBUTIONS W.W. designed experiments, fabricated and implanted the grafts, characterized explants, and analyzed data. R.A. performed mechanical characterization of grafts and explants and analyzed data. Y.W. designed experiments and supervised the project. All authors interpreted results and contributed to writing the manuscript.

low[12,13]. Interestingly, host remodeling of tissue engineered constructs post-implantation can increase elastin expression[14]. This positive remodeling suggests that the host may be a good source of cells and a more efficient “bioreactor” than the current in vitro tissue-engineering paradigm. This inspired us to fully harness the body's regenerative capacity to remodel cell-free synthetic grafts with an open porous structure that accelerates cell infiltration and remodeling (Fig. 1a). We believe that for a graft that can withstand arterial pressure, host remodeling capability is the most important criterion.

Rapid remodeling of a synthetic graft to a neo-artery will likely offer efficient integration with host tissue, a nonthrombogenic lumen, and mechanical properties matching native vessels because it reduces the duration of host exposure to foreign materials. Enabling application of synthetic vascular grafts in small diameter arteries offers multiple advantages: avoidance of donor site morbidity, bypass of in vitro cell culture, ready availability, easy storage and transport, and potentially faster clinical adoption.

To design a synthetic graft capable of rapid host remodeling, we examined the following criteria: (1) Graft material: We chose a fast degrading elastomer, poly(glycerol sebacate) (PGS), because timely degradation is essential for rapid host remodeling and mechanical conditioning is recognized as an important remodeling cue[6]. Elastomers efficiently transduce mechanical stimulation tocells. (2) Graft porosity: We chose highly porous grafts with interconnected pores to enable immediate host cell infiltration. To prevent bleeding, we enclosed grafts with a leak-proof sheath. (3) Thromboresistance: We chose heparin coating. The graft is a blood contacting foreign material prone to clotting. Clotting can occlude grafts and block cell infiltration into the graft wall. Heparin is a well-recognized standard in thromboresistance[15].

RESULTS

The open porous graft is suturable and resists platelet adhesion

Consistent with the design criteria, our graft consists of a heparin-coated porous tube wrapped with a 15 μm thin electrospun sheath (Fig. 1 b–d). The porous tube is made from PGS fabricated as previously described except a 1 mm mandrel was used[13]. The sheath is a polycaprolactone (PCL) mesh that increases graft strength and prevents bleeding by controlled fibrin formation within the sheath. Composite grafts are stored at ambient temperature. Micro-computed tomography (micro-CT) morphometric analysis indicates that the inner diameter of the graft is 720 μm, the wall thickness is 290 μm, and over 99.99 % of the pores are interconnected (Supplementary Table 1). High pore interconnectivity is critical for efficient cell infiltration,the first step in initiating host remodeling. PGS has numerous –OH groups that can form hydrogen bonds with heparin. Thus heparinization of PGS likely renders the graft lumen non-thromobogenic and inhibits excessive blood clotting within the graft wall. Heparin coating significantly reduces platelet adhesion on grafts (Fig.1 e–g). Scanning electron microscopy (SEM) reveals that heparin coating (2 mg ml^{-1}) also reduces fibrin formation, and most adhered platelets appear quiescent (Fig. 1e,f). The small pore size of the PCL sheath likely permits fibrin formation within the sheath and prevents leakage. Although very thin, the sheath significantly increases the suture retention force of the graft from 0.11 ± 0.0087 to 0.45 ± 0.031 N and is stronger than the break force of 9-0 suture (0.26

± 0.046 N) used for the microsurgical anastomosis (Fig. 1h). Furthermore, the PCL sheath increases elastic tensile modulus from 243 ± 71.8 to 536 ± 119 kPa ($P < 0.05$) and ultimate tensile strength from 76.6 ± 15.7 to 3790 ± 1450 kPa ($P < 0.001$).

Rapid graft remodeling leads to strong and compliant neo-artery

Interposition grafting of ethylene-oxide-sterilized grafts was performed in the abdominal aorta of Lewis rats (n = 21) without heparin administration during surgery or systemic heparin treatment after (Fig. 1i). The implantation immediately exposed the grafts directly to 120 mmHg pressure and an arterial hemodynamic environment. Therefore, in terms of allowing unobstructed blood flow upon implantation, the grafts performed the same function as autografts in bypass surgeries. Grafts reddened with the infiltration of blood cells but the PCL sheath effectively prevented bleeding. The host rapidly remodeled patent grafts: by 14 days, grafts were more translucent and compliant, and began to integrate with the surrounding host tissue; by 90 days, grafts were covered with fascia, closely resembled the native aorta, and were well integrated with host tissue (Supplementary Video 1).

Accompanying the visual remodeling is the pronounced change in mechanical properties. Neo-artery burst pressure is 2360 ± 673 mmHg approaching that of native aorta at 3415 ± 529 mmHg (Fig. 1j, left), and is significantly higher than that of human saphenous veins (1680 ± 307 mmHg), the most utilized autografts for coronary artery bypass surgery and lower limb vascular reconstruction[16,17]. Unimplanted grafts leak due to their high porosity and have no burst pressure to compare. Before implantation, composite grafts are stiffer than native arteries with no toe region in the stress-strain curve (Fig. 1j, middle). Host remodeling substantially altered the stress-strain curve of grafts with a clear toe region in the neo-arteries. Neo-arteries appeared softer than the native aorta, although the differences are insignificant. More importantly, the compliance of the neo-arteries (11 ± 2.2 %) is statistically the same as native aorta at 6.7 ± 2.3 % in the 80–120 mmHg range[4]. More informative than this single value of compliance is a plot of compliance over the whole pressure range (Fig. 1j, right). It is important to note that not only is the neo-artery strong, but it is also compliant. The high compliance of neo-arteries contrasts greatly with the lower compliance of unimplanted grafts, suggesting extensive graft remodeling.

This fast host remodeling is explained by widespread cell infiltration soon after implantation. The open porous structure of the graft allows extensive cell penetration into the graft wall, and nucleated cells occupied many of the pores within 3 days (Supplementary Fig. 1). Smooth muscle cells extensively infiltrate the graft within 14 days (Fig. 2a). Cells positive for α-smooth muscle actin (α-SMA), a protein specific to mural cells including smooth muscle, were widely distributed within the graft wall. Higher magnification illustrates that smooth muscle cells are not organized into circumferential layers at this early stage, but rather they are mixed α-SMA-negative cells (Fig. 2b–c). Co-staining of endothelial and smooth muscle cells indicate that the smooth muscle layer is separated from the blood by an endothelium (Fig. 2d). By 90 days the cellularity of the neo-artery might be slightly higher, but is comparable to that of native aortas (2.14 ± 0.34 vs. 1.36 ± 0.40 μg DNA mg^{-1} wet weight, $P = 0.06$). Brightfield images reveal a band of dark spots mixed

with cells located generally closer to the lumen. This acellular matter is likely remnants of graft materials that are visible as dark fibers in brightfield images (Supplementary Fig. 2).

Profound graft remodeling is also reflected at the tissue level in histological observations. Within 14 days grafts experience extensive degradation (Fig. 3a–b) while cells synthesize substantial ECM (Fig. 3b). Therefore, remodeled grafts withstand arterial pressure despite substantial graft degradation. The luminal area of the graft and the native aorta remains statistically the same throughout remodeling, suggesting absence of aneurysm and stenosis (Fig. 3c). The thickness of the graft wall decreases over time but is still thicker than the native aorta at 90 days. The majority of the graft resembles native arteries albeit the ECM fibers are less dense and less organized. Both the difference in wall thickness and ECM fiber density demonstrate that progressive remodeling of the graft is still active at 3 months.

Macrophages actively participate in the remodeling of the graft: a band of inflammatory cells including newly recruited macrophages ($CD68^+$) is visible beneath the lumen at 14 days. At 28 days, macrophages are distributed more evenly throughout grafts at a lower density than 14 days (Fig. 3d–f). At 90 days, most of the inflammatory response is resolved with only a small area of the neo-artery positive for macrophages. This trend correlates with the disappearance of the putative graft materials (Supplementary Fig. 2). Macrophages are heterogeneous with pro-inflammatory (M1) and several alternatively activated (M2) subclasses[18,19]. Positive staining of CD163 suggests the presence of M2 macrophages that are generally accepted as anti-inflammatory and facilitate constructive remodeling[20].

Smooth muscle cells are important for blood vessel function. Immuofluorescent staining revealed the presence of smooth muscle cells within 14 days and a progressively more organized media layer (Fig. 3g–h). Strong expression of myosin heavy chain indicates a contractile smooth muscle phenotype in neo-arteries (Fig. 3h). Myosin heavy chain is a late stage differentiation marker for smooth muscle. We only found one previous report on positive myosin heavy chain staining in vascular grafts[21]. Neo-arteries stain positive for fibroblast surface protein in the outer layer at 90 days, suggesting the formation of an adventitia-like tissue (Supplementary Fig. 3). Layers are distinct, resembling the trilaminar structure of a muscular artery.

The significant impact of host cells on the graft is further revealed in ECM composition. The neo-artery wall contains significant amounts of elastin, collagen I and III, and glycosaminoglycans (Fig. 4a). The amount of elastin in the neo-artery at 90 days is 77 % and total collagen is statistically the same as native aorta (Fig. 4b). These ECM macromolecules align circumferentially, mimicking their orientation in native arteries. However, native matrix is more compact and less cellular than in the neo-artery. Nonetheless, high ECM production provides a molecular explanation on the observed match of mechanical properties between the neo-artery and the host aorta.

Endothelialized neo-artery pulses synchronously with host aorta

Integration with host tissue is often a major challenge in tissue engineering. Laser Doppler ultrasound imaging of grafts indicates excellent patency and strong, synchronous pulsation with host aorta (Fig. 5a and Supplementary Video 1). Regular and clear pulsation of neo-

arteries indicates excellent integration with host tissue. To the best of our knowledge, this is the first report of any vascular graft that pulses with host arteries. The high patency is corroborated by angiography (Fig. 5b). This correlates well with a confluent endothelium that transitions smoothly from neo-artery to host aorta. The transition is only marked by the suture (Fig. 5c). Von Willebrand factor (vWF) staining revealed a confluent endothelial monolayer covering of the lumen (Fig. 5d,e). Basement membrane separates the endothelial from the smooth muscle layer as indicated by transmission electron microscopy (Fig. 5f). Basement membrane prevents smooth muscle cell migration to the endothelial layer, thereby preventing intimal hyperplasia[22].We found no evidence of intimal hyperplasia in neo-arteries. In the 4 observed cases of graft occlusion (4/21; 19.0 %) the cause was acute anastamotic thrombosis in 3 cases where the animals died. Acute thrombosis was also suspected in one rat that survived with an occluded graft because no graft remodeling was observed in the explant (Supplementary Fig. 4). Acute thrombosis is likely due to endothelial injury at the anastomosis in the absence of systemic anticoagulation. Overall patency as determined by ultrasonography, angiography and necropsy was 80.9 % (17/21) with time points of up to 90 days. Patency rates were 60 % (3/5), 100 % (5/5), and 81.8 % (9/11) for grafts explanted for days 14, 28, and 90, respectively. This overall graft patency is similar to a previous report of an antithrombogenic vascular graft[7].

Graft material is of critical importance to host remodeling. When PCL tubes substituted PGS tubes with all other graft parameters being identical, graft remodeling was substantially impaired (Supplementary Fig. 5): Only a thin layer of smooth muscle was observed near the lumen. This is consistent with results of other cell-free approaches in arterial tissue engineering where a thin layer of endothelial cells and small amount of smooth muscle were present with graft materials largely intact. Cells within the interstitial space of the graft wall were α-SMA-negative and were potentially inflammatory cells or fibroblasts. PCL grafts exhibited poor integration with host tissue even at 90 days where a clear boundary was visible and the grafted segment distorted the aorta (Supplementary Fig. 6). Interestingly, collagen I expression was much higher than collagen III and elastin. Collagen I distribution was extensive, spanning the whole graft area from lumen to albumen (outer surface), whereas other ECM proteins were mostly expressed only near the lumen. Coupling this with the “walled-off” appearance of the H&E stained graft suggests that collagen I might serve to isolate the PCL from the host.

DISCUSSION

Cell-free approaches to tissue engineering are still provocative and scarce with a focus on slow degrading polymers. A 1 mm polylactide graft was successfully endothelialized in rats and 10 mm composite polylactide-polyglycolide grafts showed good patency in canine and porcine models. However, grafts degraded slowly, limiting cell penetration and causing prolonged presence of foreign materials. Additionally, no compliance data or ECM content were reported[7,23,24]. Porcine small intestinal submucosa (SIS) grafts demonstrated variable patency above 3 mm diameter[25–28], but smaller grafts failed by acute thrombosis despite heparin soaking and systemic heparinization.[29] A 4 mm graft based on SIS was populated by endothelial and smooth muscle cells by 3 months in rabbits[30]. However, no mechanical data or ECM content were reported, and the bradykinin vaso-response was counter-

physiologic. Poly(ester urethane)urea elastomeric grafts were recently shown to be populated by endothelial and smooth muscle cells[31]. Grafts contained both collagen and elastin, but the graft material appeared largely intact at 6 months. A PCL and hydroxyapatite scaffold infused with growth factors regenerated the articular surface of rabbit cartilage[32], however, resorption of hydroxyapatite is very slow.

Our philosophy departs from the above in that we emphasize rapid graft degradation and host remodeling. To the best of our knowledge, the utilization of fast degrading synthetic grafts is a new design perspective to vascular substitutes. This report is the first step that shows promising results with a nearly complete host remodeling and good integration within 3 months. We believe three features of the reported graft are important: fast degradation, mechanical properties, and pore size. We suspect that rapid graft degradation is the most critical because it likely induces different inflammatory responses from long-lasting materials. Rapid degradation progressively generates more space for cell infiltration, proliferation, and matrix production. Furthermore, fast degradation reduces the duration of host exposure to foreign material. Long-lasting materials cause tissue stiffening from fibrous encapsulation, and can activate inflammatory cells to induce neointimal hyperplasia[33]. Matching mechanical properties and optimizing graft pore size may further promote host remodeling and integration. Matching arterial mechanical properties likely promotes vascular cell differentiation and avoids stress shielding[34]. PGS is the primary component of our grafts, and its modulus is close to that of native aortas (148 ± 55 vs. 390 ± 191 kPa) at the strains experienced by new grafts over 80 to 120 mmHg. Small pores in our grafts likely pack infiltrating cells close together to promote self-assembly[13].

As with any new technology, many questions remain to be answered. The applicability of this approach in large animals awaits investigation. Rats also have different regeneration potential and a greater capacity to endothelialize vascular grafts than humans (especially aged humans)[35,36]. It is important to investigate the rate of graft endothelialization and the safety of surgeries with no or low heparin in large animals. The animals we used are healthy animals because of the lack of atherosclerotic animals with suitable artery sizes. Up to now, only ApoE$^{-/-}$ mice are available and widely accepted.

The type and quantity of cells recruited to the graft and their changes over time remains to be studied. vWF- and α-SMA-negative cells in the neo-artery wall at 14 days may be a mixture of progenitor and inflammatory cells. Macrophages play a critical role in vascular graft remodeling[8,37]. A substantial fraction of infiltrating macrophages in our grafts expressed M2 macrophage marker CD163. Hibino *et al.* found that mouse vena cava grafts with higher M2 activation stenosed more[37]. In contrast, none of our grafts demonstrated stenosis even at 90 days. This could be due to the difference in graft material and design or differences in animal models. A large number of smooth muscle cells are present in the neo-artery wall. Tracing their origin may reveal how to accelerate their recruitment. Progenitor cells in the adventitia of the vena cava and the fascia could facilitate regeneration via paracrine effects or contribute directly to the regeneration of the neo-artery. Consequently, parts of grafts contacting the cava and fascia might form a thicker wall more rapidly, accounting for the non-uniform thickness of neo-arteries (Fig. 3a).

In addition to increasing anti-thrombogenicity, heparin is known to bind, stabilize, and potentiate the activity of a wide variety of bioactive molecules[38]. Heparin could localize FGF and VEGF families of angiogenic factors to grafts, promoting vascular cell infiltration. Heparin may also promote cellular infiltration by binding cell adhesion proteins such as PECAM-1 and L-selectin, adhesive matrix proteins, and chemokines[38]. Previous work demonstrated that heparinization improves implant cellularity and angiogenesis[39]. Heparin can also promote remodeling by binding remodeling factors such as tissue plasminogen activator[38].

PCL improves graft suturability, however it might not be the optimal sheath material. Residues of graft materials observed at 3 months are likely PCL because solid non-porous PGS degrades within 2 months subcutaneously[40]. The presence of graft material when the neo-artery is sufficiently strong and compliant likely inhibits host remodeling. Thus investigation of sheath materials with mechanical properties similar to PCL but with a faster degradation is warranted. This research may lead to advanced biomaterials and graft designs that can bring synthetic small arterial grafts closer to clinical translation. Furthermore, the focus on rapid graft remodeling is likely applicable to tissues other than blood vessels, especially when combined with progenitor-cell homing signals.

METHODS

Graft fabrication

To fabricate the PGS core we used a modified salt fusion and leaching method as previously described except that we used a 1 mm mandrel and a 1.25 mm outer mold[13]. To fabricate the PCL sheath we dissolved PCL (M_n 80 kDa, Aldrich) in 2,2,2-trifluoroethanol (ACROS) at 14 % w v^{-1} and electrospun the solution onto the rotating PGS-salt template (20 rpm). Immersion in deionized water removed salt from PCL-PGS-salt composites. We lyophilized the grafts (Labconco Freezone 4.5) and stored them in a desiccator at ambient temperature. We used ethylene oxide to sterilize grafts.

Graft characterization

Mechanical testing—To measure elastic modulus and suture retention strength of grafts we used an electromechanical testing machine (Insight, MTS Systems) with a 5.0 N load cell. We measured tensile strength and elastic modulus as previously described with some modification (detailed in supplementary methods)[13]. We took ultimate tensile strength as the peak stress of the stress-strain curve. To measure suture retention strength, we placed a 7–0 prolene suture 1 mm from the end of each graft. We fixed suture around the upper hook and immobilized the grafts in the lower hook. We measured the force needed to pull suture apart from the graft using a crosshead speed of 2 mm min^{-1}. To evaluate whether suture retention met the microsurgical requirement we measured the break forces of 9–0 sutures.

SEM, micro-CT, and platelet adhesion quantification are detailed in supplementary methods.

Animal studies

Implantation—Animals were cared for in compliance with protocols approved by the Committee on Animal Care of the University of Pittsburgh following NIH guidelines for the care and use of laboratory animals (NIH publication No. 85–23 rev. 1985). We used male Lewis rats (body weight: 200–250g, Charles River Laboratories, Boston, MA) for animal experiments. We successfully implanted 27 rats with either PGS based composite grafts (n = 21) or porous grafts made completely from PCL (n = 6). Surgical survival rate was 87.5% (21/24). Three rats died during surgery due to bleeding from aortic or inferior vena cava injury, and we excluded these from animal counts. We performed interpositional implantation in rat abdominal aorta as follows: A midline abdominal incision exposed the abdominal aorta in rats anesthetized by isoflurane inhalation. To implant the graft we separated the aorta from the inferior vena cava, cross-clamped the infrarenal abdominal aorta, transected a 4 mm segment, and inserted the composite graft (8–10 mm in length) in the gap. End to end anastomosis connected grafts to the native aorta with 9–0 nylon suture. Animals received no postoperative anti-coagulation or anti-platelet treatment. We explanted grafts at 14 days (n = 5), 28 days (n = 5) and 90 days (n = 11) post-implantation. We sacrificed all rats implanted with PCL-only grafts (n = 6) at 90 days.

X-ray angiography and Doppler ultrasound examination—To detect blood flow in grafts we used Doppler ultrasound monthly and X-ray angiography immediately prior to explantation. Details are in supplementary methods.

Biochemical Evaluation

To quantify elastin, collagen, and DNA content of regenerated and native arteries, we used a Fastin Elastin Assay kit (F2000; Biocolor), Sircol™ Collagen Assay (MP Biomedicals), and DNeasy Blood and Tissue Kit (Qiagen) according to manufacturer instructions (detailed in supplementary methods).

Mechanical Characterization

Compliance and Tensile Elastic Modulus—To prepare aortic segments (1 cm length) for testing, we trimmed off connective tissue and sealed branching vessels with 7–0 suture. We then strained segments longitudinally to 10 % and pressurized by infusing with physiologic saline solution (PSS) using a syringe pump (NE-1000, New Era Pump Systems). To precondition we cycled aortas between 0 and 130 mmHg until we acquired reproducible diameter vs. pressure curves. We calculated compliance and modulus from the last cycle. A pressure transducer (PX309 Omegadyne), optical micrometer (LS7070, Keyence), and data acquisition system (PowerLab 8/30, AD Instruments) recorded pressure and diameter synchronously. Description of compliance and modulus derivations from diameter vs. pressure data is in supplementary methods.

Statistical Analysis

A two-tailed Student's *t* test made comparisons between two groups. A one way ANOVA followed by Tukey's HSD post-hoc test made comparisons between three or more groups.

We confirmed normal distribution of data and homogeneity of variance between groups using IBM SPSS Statistics 19.

A more detailed description of SEM, micro-CT, platelet adhesion quantification, X-ray angiography and Doppler ultrasound examination, histology, immunofluorescent staining, biochemical evaluation, and explant mechanical characterization is available in supplementary methods.

Supplementary Material

Refer to Web version on PubMed Central for supplementary material.

ACKNOWLEDGEMENTS

This research is supported by a US National Institutes of Health grant HL089658, American Heart Association award 0730031N, US National Institutes of Health training grant 2T32HL076124. We thank S. Shroff for insightful discussions on mechanical testing of arteries, W. Wagner for access to the laser Doppler ultrasound, and K. Kim for assistance with ultrasound imaging. We greatly appreciate R. Wagner and D. Rossi for performing angiography, M. Witt for DNA quantification, and D. Stolz, M. Sun and D. Clay for performing TEM.

REFERENCES

1. Weinberg CB, Bell E. A blood vessel model constructed from collagen and cultured vascular cells. Science. 1986; 231:397–400. [PubMed: 2934816]
2. Niklason LE, et al. Functional arteries grown in vitro. Science. 1999; 284:489–493. [PubMed: 10205057]
3. Dahl SL, et al. Readily available tissue-engineered vascular grafts. Sci Transl Med. 2011; 3:1–11.
4. L'Heureux N, et al. Human tissue-engineered blood vessels for adult arterial revascularization. Nat. Med. 2006; 12:361–365. [PubMed: 16491087]
5. Kaushal S, et al. Functional small-diameter neovessels created using endothelial progenitor cells expanded ex vivo. Nat. Med. 2001; 7:1035–1040. [PubMed: 11533707]
6. Isenberg BC, Williams C, Tranquillo RT. Small-diameter artificial arteries engineered in vitro. Circ Res. 2006; 98:25–35. [PubMed: 16397155]
7. Hashi CK, et al. Antithrombogenic modification of small-diameter microfibrous vascular grafts. Arterioscler Thromb Vasc Biol. 2010; 30:1621–1627. [PubMed: 20466974]
8. Roh JD, et al. Tissue-engineered vascular grafts transform into mature blood vessels via an inflammation-mediated process of vascular remodeling. Proc Natl Acad Sci U S A. 2010; 107:4669–4674. [PubMed: 20207947]
9. He W, et al. Pericyte-based human tissue engineered vascular grafts. Biomaterials. 2010; 31:8235–8244. [PubMed: 20684982]
10. Neff LP, et al. Vascular smooth muscle enhances functionality of tissue-engineered blood vessels in vivo. J Vasc Surg. 2011; 53:426–434. [PubMed: 20934837]
11. Zhu C, et al. Development of anti-atherosclerotic tissue-engineered blood vessel by A20-regulated endothelial progenitor cells seeding decellularized vascular matrix. Biomaterials. 2008; 29:2628–2636. [PubMed: 18377984]
12. Long JL, Tranquillo RT. Elastic fiber production in cardiovascular tissue-equivalents. Matrix Biol. 2003; 22:339–350. [PubMed: 12935818]
13. Lee KW, Stolz DB, Wang Y. Substantial expression of mature elastin in arterial constructs. Proc Natl Acad Sci U S A. 2011; 108:2705–2710. [PubMed: 21282618]
14. L'Heureux N, McAllister TN, de la Fuente LM. Tissue-engineered blood vessel for adult arterial revascularization. N Engl J Med. 2007; 357:1451–1453. [PubMed: 17914054]
15. Damus PS, Hicks M, Rosenberg RD. Anticoagulant action of heparin. Nature. 1973; 246:355–357. [PubMed: 4586320]

16. L'Heureux N, Paquet S, Labbe R, Germain L, Auger FA. A completely biological tissue-engineered human blood vessel. FASEB J. 1998; 12:47–56. [PubMed: 9438410]
17. Veith FJ, et al. Six-year prospective multicenter randomized comparison of autologous saphenous vein and expanded polytetrafluoroethylene grafts in infrainguinal arterial reconstructions. J Vasc Surg. 1986; 3:104–114. [PubMed: 3510323]
18. Ricardo SD, van Goor H, Eddy AA. Macrophage diversity in renal injury and repair. J Clin Invest. 2008; 118:3522–3530. [PubMed: 18982158]
19. Mantovani A, Garlanda C, Locati M. Macrophage diversity and polarization in atherosclerosis: a question of balance. Arterioscler Thromb Vasc Biol. 2009; 29:1419–1423. [PubMed: 19696407]
20. Brown BN, Valentin JE, Stewart-Akers AM, McCabe GP, Badylak SF. Macrophage phenotype and remodeling outcomes in response to biologic scaffolds with and without a cellular component. Biomaterials. 2009; 30:1482–1491. [PubMed: 19121538]
21. Hashi CK, et al. Antithrombogenic property of bone marrow mesenchymal stem cells in nanofibrous vascular grafts. Proc. Natl. Acad. Sci. U.S.A. 2007; 104:11915–11920. [PubMed: 17615237]
22. Turner NA, Hall KT, Ball SG, Porter KE. Selective gene silencing of either MMP-2 or MMP-9 inhibits invasion of human saphenous vein smooth muscle cells. Atherosclerosis. 2007; 193:36–43. [PubMed: 16979647]
23. Torikai K, et al. A self-renewing, tissue-engineered vascular graft for arterial reconstruction. J Thorac Cardiovasc Surg. 2008; 136:37–45. 45, e31. [PubMed: 18603051]
24. Yokota T, et al. In situ tissue regeneration using a novel tissue-engineered, small-caliber vascular graft without cell seeding. J Thorac Cardiovasc Surg. 2008; 136:900–907. [PubMed: 18954628]
25. Pavcnik D, et al. Angiographic evaluation of carotid artery grafting with prefabricated small-diameter, small-intestinal submucosa grafts in sheep. Cardiovasc Intervent Radiol. 2009; 32:106–113. [PubMed: 18931872]
26. Sandusky GE, Lantz GC, Badylak SF. Healing comparison of small intestine submucosa and ePTFE grafts in the canine carotid artery. J Surg Res. 1995; 58:415–420. [PubMed: 7723321]
27. Sandusky GE Jr. Badylak SF, Morff RJ, Johnson WD, Lantz G. Histologic findings after in vivo placement of small intestine submucosal vascular grafts and saphenous vein grafts in the carotid artery in dogs. Am J Pathol. 1992; 140:317–324. [PubMed: 1739125]
28. Lantz GC, Badylak SF, Coffey AC, Geddes LA, Blevins WE. Small intestinal submucosa as a small-diameter arterial graft in the dog. J Invest Surg. 1990; 3:217–227. [PubMed: 2078544]
29. Prevel CD, et al. Experimental evaluation of small intestinal submucosa as a microvascular graft material. Microsurgery. 1994; 15:586–591. discussion 592–583. [PubMed: 7830542]
30. Huynh T, et al. Remodeling of an acellular collagen graft into a physiologically responsive neovessel. Nat Biotechnol. 1999; 17:1083–1086. [PubMed: 10545913]
31. Soletti L, et al. In vivo performance of a phospholipid-coated bioerodable elastomeric graft for small-diameter vascular applications. J Biomed Mater Res A. 2011; 96:436–448. [PubMed: 21171163]
32. Lee CH, et al. Regeneration of the articular surface of the rabbit synovial joint by cell homing: a proof of concept study. Lancet. 2010; 376:440–448. [PubMed: 20692530]
33. Li L, Terry CM, Shiu YT, Cheung AK. Neointimal hyperplasia associated with synthetic hemodialysis grafts. Kidney Int. 2008; 74:1247–1261. [PubMed: 18668026]
34. Discher DE, Janmey P, Wang YL. Tissue cells feel and respond to the stiffness of their substrate. Science. 2005; 310:1139–1143. [PubMed: 16293750]
35. Zilla P, Bezuidenhout D, Human P. Prosthetic vascular grafts: wrong models, wrong questions and no healing. Biomaterials. 2007; 28:5009–5027. [PubMed: 17688939]
36. Bull DA, et al. Cellular origin and rate of endothelial cell coverage of PTFE grafts. J Surg Res. 1995; 58:58–68. [PubMed: 7830407]
37. Hibino N, et al. A critical role for macrophages in neovessel formation and the development of stenosis in tissue-engineered vascular grafts. FASEB J. 2011
38. Bernfield M, et al. Functions of cell surface heparan sulfate proteoglycans. Annu Rev Biochem. 1999; 68:729–777. [PubMed: 10872465]

39. Bezuidenhout D, et al. Covalent surface heparinization potentiates porous polyurethane scaffold vascularization. J Biomater Appl. 2010; 24:401–418. [PubMed: 19033329]

40. Wang Y, Kim YM, Langer R. In vivo degradation characteristics of poly(glycerol sebacate). J Biomed Mater Res A. 2003; 66:192–197. [PubMed: 12833446]

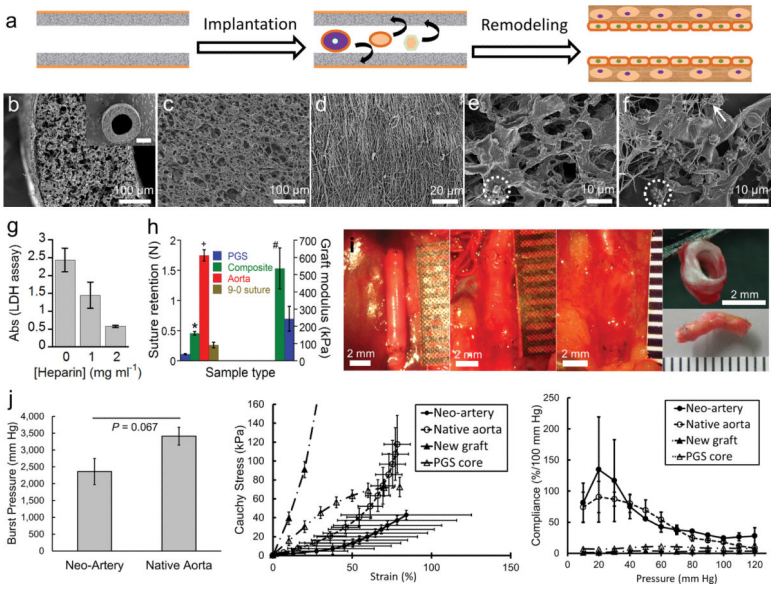

Figure 1.

Characterization of the composite graft and host remodeling of the graft *in vivo*. (**a**) Schematic representation of direct implantation of the cell-free graft and the proposed remodeling process of the graft into a biological neo-artery. (**b**) SEM images of composite grafts to show surface topology, scale bar 100 μm. Inset: top view of the graft, scale bar 500 μm. (**c**) Lumen of the PGS tube, scale bar 100 μm. (**d**) The PCL fibrous sheath, scale bar 20 μm. (**e**) SEM of heparin soaked PGS after incubation in platelet rich plasma to show platelet adhesion and fibrin deposition. Scale bar 10μm. (**f**) SEM of unheparinized PGS after incubation in platelet rich plasma, scale bar 10 μm. An adherent platelet is circled in **e** and **f** to highlight difference in platelet morphology. Arrow indicates fibrin in (**f**). (**g**) Platelet adhesion on PGS presoaked in varying heparin concentrations, quantified by lactate dehydrogenase assay (n = 5). $P < 0.0001$ between all groups. (**h**) Suture retention and elastic moduli of grafts. Break force of 9–0 suture indicated by &. $P < 0.05$: * composite graft vs. 9–0 suture,$^{+}$ composite graft vs. rat aorta, # composite graft modulus (n = 8) vs. that of PGS (grafts without the PCL sheath, n = 3). n = 5 for other groups. (**i**) Gross appearance of the graft during host remodeling to assess integration with host tissue. From left to right: day 0, day 14, day 90, and day 90 (top and bottom). Scale bars 2 mm, all ruler ticks 1 mm. Non-degradable sutures (black) mark the graft location. (**j**) Mechanical properties of neo-arteries. Left: The burst pressure of the neo-artery (n = 3) is statistically the same as native aorta (n = 4). Middle: Stress-strain curves of arteries and new grafts. “New grafts” represents unimplanted composite grafts. “PGS core” represents new grafts without the PCL sheath. Right: Compliance of arteries and new grafts. Standard errors for new grafts and the PGS core are very small and barely visible at the plotted scale. For **j**, n = 3 for neo-arteries and n = 4 for native aortas, new grafts, and PGS cores. Data represent mean ± standard deviation for **e**–**g** and mean ± standard error for **j.**

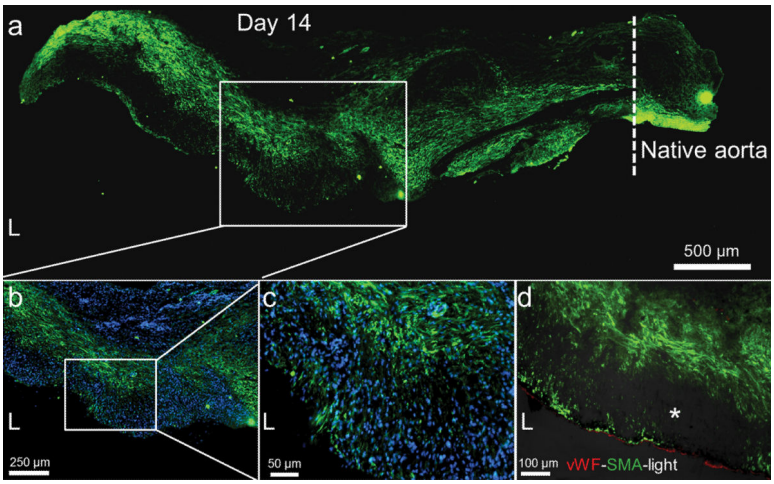

Figure 2.

Smooth muscle cell infiltration and organization at 14 days. (**a**) Smooth muscle cell distribution (α-SMA, green) within the remodeled graft wall. The tissue was split longitudinally, half of which is shown. Native aorta is on the right, its border with the graft is indicated by the dashed line, scale bar 500 μm. L = lumen. (**b**) Magnified view of the mid-graft shows distribution of both α-SMA positive (green) and α-SMA negative cells. Nuclei counterstained by DAPI, scale bar 250 μm. (**c**) Further magnification of the mid-graft to view the complicated smooth muscle cell distribution (α-SMA, green), scale bar 50 μm. (**d**) Distribution of endothelial cells (vWF, red) and smooth muscle cells (α-SMA, green) in the graft wall. Immunofluorescent images merged with the brightfield image (darkened so as not to overwhelm the fluorescent images). Dark spots (*) in the brightfield image might be residual graft material. Scale bar 100 μm. brightfield images of original brightness are in Supplementary Fig. 2.

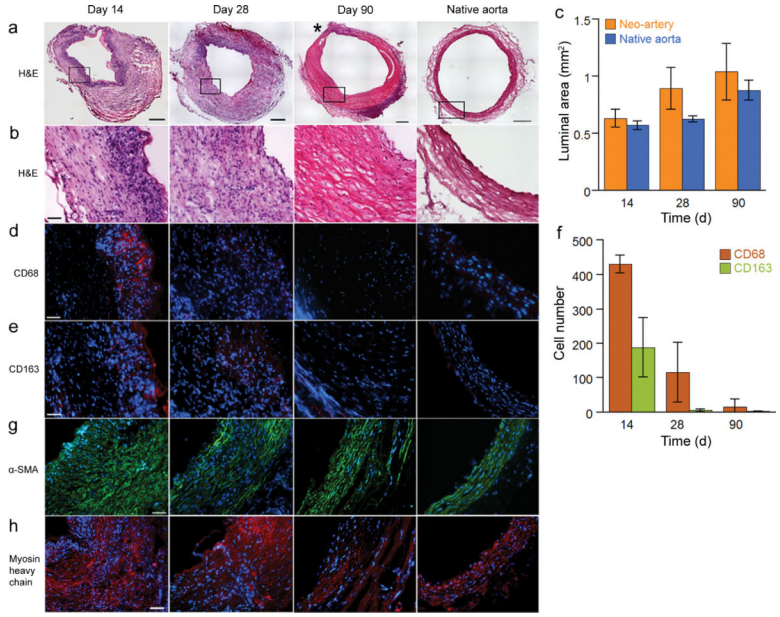

Figure 3.

Remodeling of grafts. (**a**) H&E staining of the grafts during the transition into a neo-artery. An area of the neo-artery wall containing inflammatory cells is marked by (*). The top of the 14-day sample was trimmed to remove the adjoining vein. Image merged from a panel of 100 μ micrographs, scale bar 250 μm. (**b**) Magnified view of the vessel wall shows ECM content and alignment, scale bar 50 μm. (**c**) Luminal area of remodeling grafts to assess stenosis and aneurysm formation. There is no statistical difference between the two groups. (**d**) Changes in number and organization of macrophages (CD68, red). (**e**) Distribution of M2 macrophages (CD163, red). (**f**) Number of CD68 and CD163 positive cells quantifies total macrophage number and the proportion of M2 macrophages. (**g**) Changes of smooth muscle cell (α-SMA, green) organization over time. (**h**) Distribution of contractile smooth muscle cells (myosin heavy chain, red). All the immuofluorescent micrographs were counterstained for nuclei by DAPI (blue), scale bar 50 μm. Data represent mean ± standard deviation for **c** and **f.**

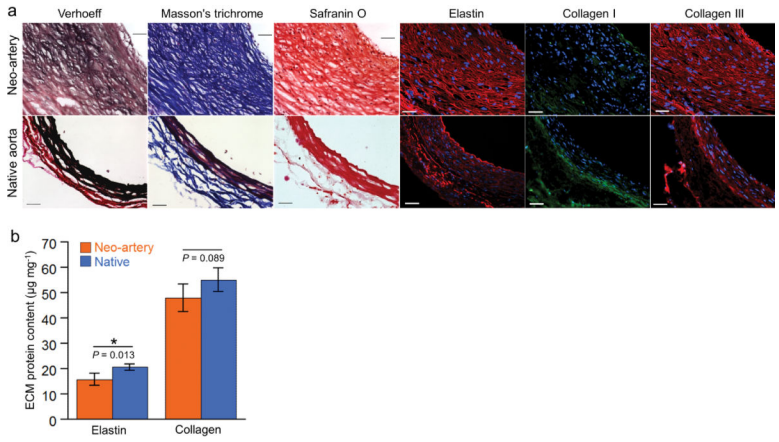

Figure 4.

ECM organization and quantification at 90 days. (**a**) Verhoeff's, Masson's trichrome, and safranin O staining show elastin (black), collagen (blue), and glycosaminoglycansin (red). Immunofluorescent staining shows distribution of elastin (red), collagen I (green), and collagen III (red). Top: day 90 explant, bottom: native aorta. (**b**) Quantification of elastin (n = 4) and total collagen (n = 4). Data represent mean ± standard deviation.

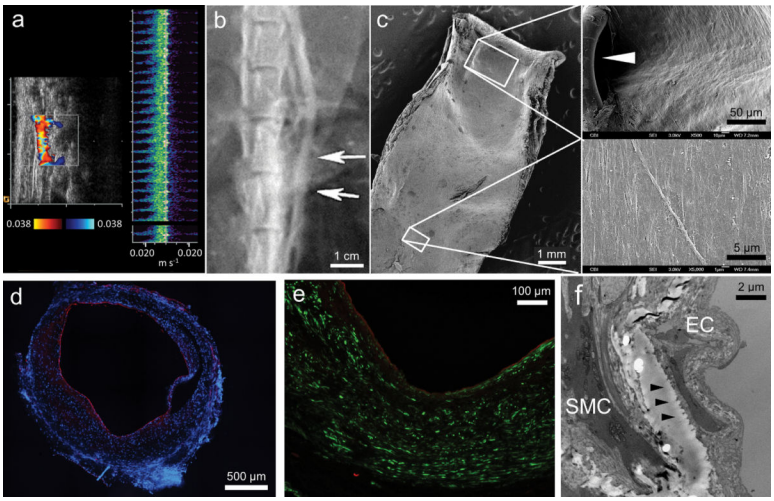

Figure 5.

Endothelialization of the neo-artery and vascular patency at day 90. (**a**) Laser Doppler ultrasound imaging assessment of graft patency and synchronization of pulsation with adjacent host aorta. Synchronization of pulsation also shown in Supplementary Video 1. (**b**) Angiography assessment of graft patency. Arrows indicate the graft location. (**c**) SEM of day 90 explant. Vessel split longitudinally, scale bar, 1 mm. Higher magnification micrographs (right) show lumenal surface at the anastomosis (suture indicated by the arrowhead, scale bar, 50 μm) and mid-graft (scale bar 5 μm). (**d**) Coverage of lumen by endothelial cells (vWF, red). Nuclei counterstained by DAPI (blue), scale bar, 500 μm. (**e**) Distribution of endothelial cells (vWF, red) and smooth muscle cells (α-SMA, green), scale bar 100 μm. (**f**) Transmission electron microscopy of interface between endothelial cells (EC) and smooth muscle cells SMC. Arrowheads denote a basement membrane. Scale bar 2 μm.